50-GHz Passively Mode-Locked Surface-Emitting Semiconductor Laser With 100-mW Average Output Power

Dirk Lorenser, Deran J. H. C. Maas, Heiko J. Unold, Aude-Reine Bellancourt, Benjamin Rudin, Emilio Gini, Dirk Ebling, and Ursula Keller, *Senior Member, IEEE*

***Abstract*—We have developed a passively mode-locked optically-pumped vertical-external-cavity surface-emitting semiconductor laser (VECSEL) which delivers up to 100 mW of average output power at a repetition rate of 50 GHz in nearly transform-limited 3.3-ps pulses at a wavelength around 960 nm. The high-repetition-rate passive mode locking was achieved with a low-saturation-fluence semiconductor saturable absorber mirror (SESAM) incorporating a single layer of quantum-dots. The output power within a nearly diffraction-limited beam was maximized using a gain structure with a low thermal impedance soldered to a diamond heat spreader. In addition, we systematically optimized the laser resonator to accommodate for the strong thermal lens caused by the optical pumping. We measured the thermal lens dioptric power and present a numerical model which is in good agreement with the measurements and is useful for optimizing resonator designs. The experimental setup is very versatile and its design and construction are discussed in detail.**

***Index Terms*—Mode locking, pulsed lasers, semiconductor lasers, thermal lens.**

I. Introduction

THE optically-pumped passively mode-locked vertical-external-cavity surface-emitting semiconductor laser (VECSEL [1]) is capable of delivering multigigahertz pulse trains with good pulse quality close to the transform limit in a diffraction-limited output beam and high average output power. After the first demonstration of passive mode locking of a VECSEL in 2000 [2] using a semiconductor saturable absorber mirror (SESAM [3], [4]), a period of rapid progress followed during which the great flexibility in design and fabrication of the semiconductor gain structure and absorber was exploited to reach watt-level average output powers [5], [6] or subpicosecond pulse durations [7].

All of this early work was done at repetition rates in the regime of 1–10 GHz. Progress towards higher repetition rates was initially slow, with a 15-GHz electrically pumped VECSEL [8] setting the reference for quite some time, but with only a few milliwatts of output power. A breakthrough occurred only very recently with the development of quantum-dot SESAMs (QD SESAMs). Their lower saturation fluence (F_{sat}) supports stable mode locking even at the lower pulse energies in high-repetition-rate lasers. The first successful experiments already resulted in new record-high pulse repetition rates in the regime of 20 and 30 GHz [9].

Even more importantly, all these results using QD SESAMs were obtained in cavity configurations with identical laser mode areas in gain and absorber. This demonstrated the feasibility of integrating such absorbers into the gain structure, which would lead to a new class of ultracompact monolithic passively mode-locked semiconductor lasers which can be fabricated cost-effectively by wafer-scale mass production. With an eye on the 100-GHz mark, the integration of a low-F_{sat} absorber into a gain structure has now become an attractive endeavor for application-oriented research in the field of semiconductor lasers. For example, applications such as optical clocking of highly integrated circuits would benefit from pulse repetition rates that can be scaled from 40 GHz to 100 GHz with at least 100 mW of average output power using the same wafer-scale technology [10], [11].

Before the full wafer-scale integration we were interested in demonstrating further pulse repetition rate scaling using the conventional concept which is based on a separate gain structure and a low-F_{sat} SESAM as discrete components in a compact folded cavity. In this paper, we report on such a passively mode-locked VECSEL with a record-high repetition rate of 50 GHz and an average power level of 100 mW. This result approaches the mechanical limits of this conventional concept.

The paper is divided into several sections. In Section II, we describe the experimental setup. Before mode locking the laser, a substantial amount of effort was invested in the optimization of the 50-GHz cavity in continuous-wave (cw) operation for maximum output power in a single transverse mode. This included a measurement of the dioptric power of the thermal lens, which is described in Section III. In Section IV, we present a numerical model of the thermal lens and compare the calculated values with the measured data. Then, in Section V, we discuss the mode locking experiments and present our best result. In Section VI, we draw conclusions from our results and observations and put them into perspective with regard to future developments.

II. Experimental Setup

A. Optical Pump System

A special pump setup was constructed for our high-repetition-rate cavities which delivers the pump beam at a 45° angle in the

Manuscript received February 7, 2006; revised April 7, 2006. This work was supported in part by the Intel Corporation through a university sponsored research agreement, the European Network of Excellence "ePIXnet," and ETH Zurich.

D. Lorenser, D. J. H. C. Maas, H. J. Unold, A.-R. Bellancourt, B. Rudin, and U. Keller are with the Institute of Quantum Electronics, ETH Hoenggerberg, CH-8093 Zurich, Switzerland (e-mail: dirk.lorenser@alumni.ethz.ch; maas@phys.ethz.ch; unold@phys.ethz.ch; bellancourt@phys.ethz.ch; rudin@phys.ethz.ch; keller@phys.ethz.ch).

E. Gini and D. Ebling are with the FIRST Center for Micro- and Nanoscience, CH-8093 Zurich, Switzerland (e-mail: gini@first.ethz.ch; dirk.ebling@gmx.de).

Digital Object Identifier 10.1109/JQE.2006.878183

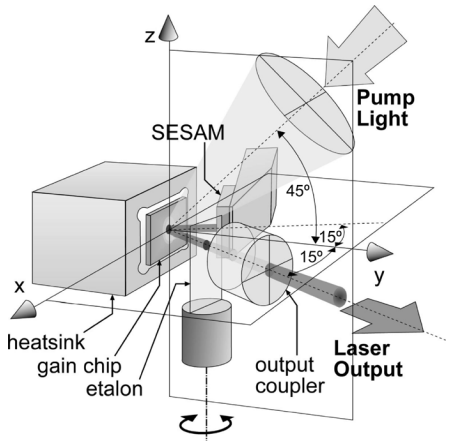

Fig. 1. Schematic illustration of the pump and cavity arrangement which was used for the 50-GHz VECSEL. The pump light is incident on the gain structure at a 45° angle in the vertical (yz) plane, which allows for a more compact cavity in the horizontal (xy) plane. The cavity has a folded V-type configuration consisting of the output coupler, the gain structure as a folding mirror, and the SESAM. The folding half-angle is 15°. An angle-tuned etalon can be inserted into the cavity.

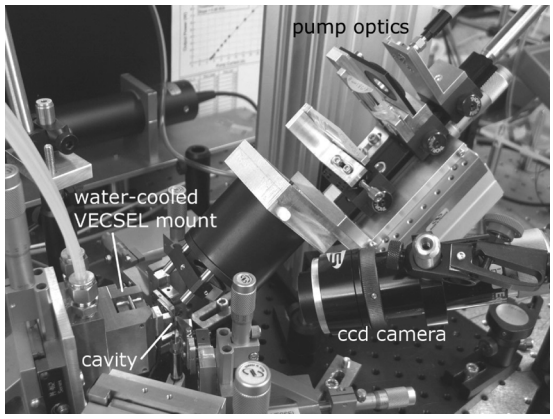

Fig. 2. Overview of the experimental setup showing the pump optics which are mounted on a 45°-tilted platform above the cavity. The end of the pump delivery fiber is visible in the upper right-hand corner. The large translation stage on the tilted platform allows to move the entire pump optics system parallel to its optical axis in order to fine-tune the position of the focal plane of the pump beam relative to the surface of the gain structure. The cavity is visible in the lower left-hand corner. The heat sink of the VECSEL gain structure is temperature-stabilized using peltier elements and a water-cooled mount.

vertical plane in order to eliminate the mechanical problem of closely packed cavity components in the horizontal plane which ultimately obstruct the passage of the pump beam. A schematic drawing of this concept is shown in Fig. 1, and a photograph of the entire experimental setup in Fig. 2. We chose a lightweight fiber-coupled pump source which can be mounted on a tilted platform elevated above the cavity. We used a commercial pump diode module capable of delivering 10 W of power at a wavelength of 808 nm in a multimode fiber with a core diameter of 100 μm and a numerical aperture (NA) of 0.22.

The details of the pump optics system are shown in Fig. 3. The two orthogonal cylindric lenses collimate the beam at different distances from the fiber end facet in the axes which lie in the vertical and horizontal planes, resulting in an elliptical beam cross section. This collimated elliptical beam is focused down using a meniscus lens and an achromatic doublet (a single

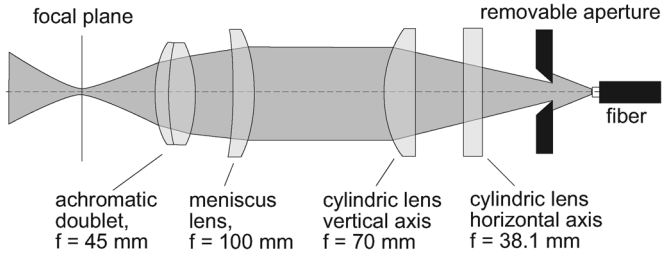

Fig. 3. Pump optics system. The beam is collimated with two orthogonal cylindric lenses at different distances from the fiber end facet to yield a collimated beam with an elliptical cross section. This beam is then focused down with the meniscus lens and the achromatic doublet.

lens would of course be sufficient, but the collimated beam diameter was too large for the available 1-in-diameter achromats, therefore the 2-in-diameter meniscus lens is used to prefocus the beam). Using this approach, we can obtain a focused spot with an ellipticity of about $\sqrt{2}$ which results in an approximately circular pump spot on the VECSEL gain structure when projected under the pump-angle of 45° (as shown in Figs. 1 and 2). We used a removable aperture to obtain a simple and quick way of changing the pump spot size without replacing lenses and doing realignment. The aperture clips part of the fiber output and therefore artificially improves the fiber NA for a better beam quality. The pump spot radius in the focus is about 65 μm with aperture inserted and about 70 μm without the aperture.

It is important to note here that the transverse pump profile obtained with this pump optics system is Gaussian-like in the focus, and the profile gradually changes in shape as one moves through the focus. This allows to fine-tune the thermal lensing by slightly shifting the focal plane of the pump optics relative to the surface of the gain structure. For this purpose, a translation stage is mounted on the elevated tilted platform (see Fig. 2) which translates the entire pump optics system (Fig. 3) parallel to its optical axis.

B. Cavity Design

A simple schematic top-down view of the cavity as well as a photograph are shown in Figs. 4 and 5. The cavity has a V-type configuration consisting of the output coupler (OC), the gain structure as a folding mirror, and the SESAM as an end mirror. Special miniaturized OCs were custom-made for this cavity. In the experiments described in the following, we used curved OCs with a curvature radius of $R = 200$ mm and a diameter of 1.2 mm, as well as flat OCs with a diameter of 2.5 mm. An etalon can be inserted into the cavity for tuning the operating wavelength of the laser and for adjusting the group-delay dispersion (GDD). It is mounted on a miniature stepper motor with a 4096:1 gearhead, enabling rotation in extremely fine increments.

C. VECSEL Gain Structure

The VECSEL gain structure used in this paper was designed for a laser wavelength around 950–960 nm and a pump wavelength of 808 nm. It consists of three main sections: a bottom mirror, an active region, and an antireflective (AR) top-section. The AlAs–$Al_{0.2}Ga_{0.8}As$ bottom mirror is a 36-pair Bragg reflector optimized for high reflectivity at the laser wavelength

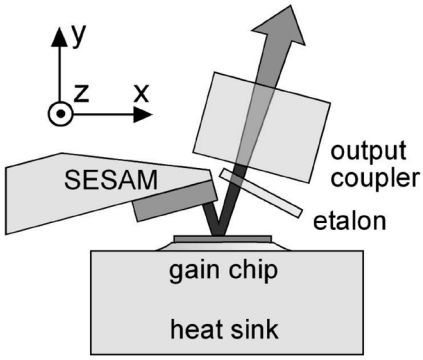

Fig. 4. Schematic drawing of the 50-GHz cavity when viewed from the top.

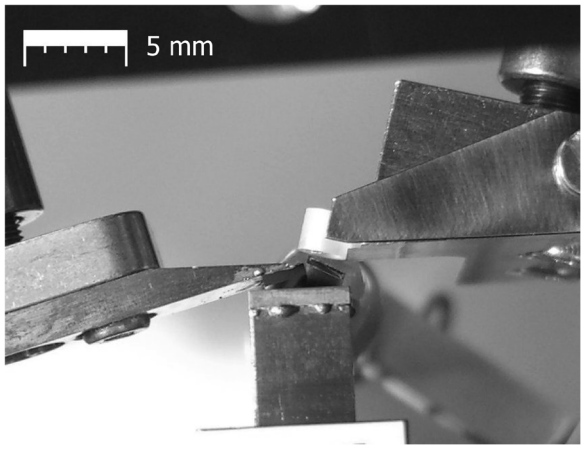

Fig. 5. Photograph of the 50-GHz cavity when viewed from the top. The total cavity length is 3 mm. The output coupler in this picture is one of the flat output couplers with a diameter of 2.5 mm. The etalon is inserted into the cavity in this picture, and the miniature stepper motor which is used to turn the etalon is visible underneath the cavity.

at normal incidence, but also for reflectivity at the pump wavelength at an angle of incidence of 45° (this results in a double-pass of the pump light through the active region). The active region contains seven $In_{0.13}Ga_{0.87}As$ quantum wells (QWs) placed in the maxima of the standing-wave pattern and separated by spacer sections made up of pump-absorbing GaAs and $GaAs_{0.94}P_{0.06}$ layers. The tensile-strained $GaAs_{0.94}P_{0.06}$ layers serve as strain-compensating layers and are positioned in the center of the spacer sections. The AlAs/$Al_{0.2}Ga_{0.8}As$ AR top section is also optimized both for the laser and the pump wavelength.

The gain structure is grown in reverse order by metal-organic vapor-phase epitaxy (MOVPE). Pieces are cleaved from the wafer, metalized with Ti–Pt–Au, and finally soldered to heat spreaders with In in a fluxless RF soldering process under vacuum. The GaAs substrate is then removed by a wet-chemical etching procedure, resulting in a very thin gain structure (thickness $\approx 7\ \mu$m) with a low thermal impedance. The design and processing of our gain structures has been described in detail in [12].

In the experiments described here, we used two gain structure samples which were cleaved from adjacent positions on the wafer. One was soldered to a lapped copper heat spreader and the other to a commercial chemical-vapor-deposition (CVD) diamond heat spreader with a thickness of 250 μm.

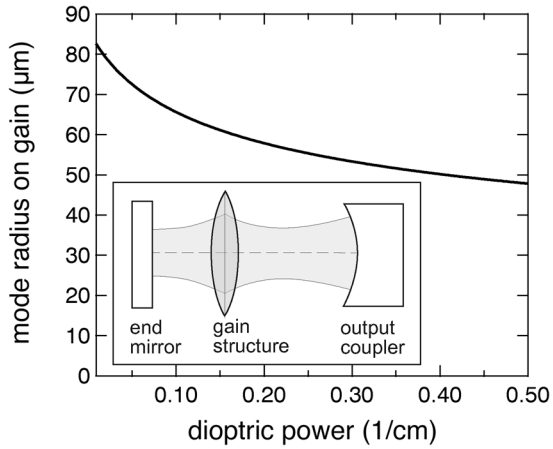

Fig. 6. Simulation of the influence of the thermal lens on the mode radius on the gain structure for a 50-GHz cavity using a curved output coupler (OC) with $R = 200$ mm. The inset shows the linear model of the cavity. The calculation was done for a wavelength of 960 nm and cavity arm lengths of 1 mm for end-mirror to gain and 2 mm for gain to OC.

III. Optimizing the CW Output Power

A. Cavity With a Curved Output Coupler

Extensive tests of the laser were performed in cw operation to optimize the output power and beam quality before attempting mode locking. The 50-GHz cavity as depicted in Fig. 4 was set up using a curved OC with $R = 200$ mm. A high-reflecting Bragg mirror was used as the end mirror instead of the SESAM, and no etalon was used. The cavity arm lengths from end mirror to gain and gain to OC were about 1 and 2 mm, respectively. The pump optics had the aperture inserted, resulting in a pump spot radius of about 65 μm. The central issue for obtaining high average output power in single-transverse mode operation is to match the laser mode size on the gain structure to the pump spot size. The very weak curvature of the OC compared to the cavity length ($R \gg L_{\mathrm{cav}}$) results in a resonator mode which is essentially a collimated Gaussian beam, with practically equal mode areas on the gain structure and the absorber. The advantages of this cavity concept for high-repetition-rate lasers in conjunction with low-F_{sat} SESAMs have been discussed in [9]. A consequence of this approach, however, is that these cavities are quite sensitive to the focusing action of the thermal lens in the gain structure. The influence of the thermal lens on the mode radius for the 50-GHz cavity is shown in Fig. 6. The calculation was done using a software based on the ray-matrix formalism for Gaussian beams [13]. One can see that the mode radius on the gain contracts as the dioptric power of the thermal lens increases (which is the case when the pump power is increased). Above a certain pump power level, the radius of the fundamental mode on the gain will become smaller than the pump spot radius and higher order transverse modes will begin to appear. A knowledge of the approximate value of the thermal lens dioptric power is, therefore, indispensable for the proper design of such cavities.

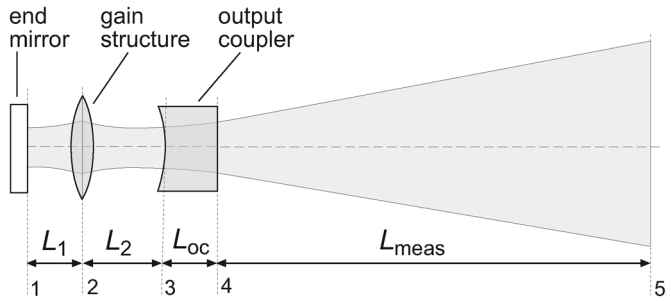

Fig. 7. Definition of the reference planes and distances involved in the measurement of the thermal lens.

The thermal lens dioptric power was determined for a range of pump powers by measuring the output beam radius of the laser with a beam profiler at a fixed distance L_{meas} from the OC. We then calculated the thermal lens which would produce such an output beam for the given optical system using the ray-matrix formalism for Gaussian beams [13].

Refer to Fig. 7 for a schematic of the optical system. If the beam radius is measured at reference plane 5, one can calculate the beam radius at reference plane 3, making use of the fact that the phase front curvature at reference plane 3 is equal to the curvature radius R of the output coupler. By propagating the beam from reference plane 3 to reference plane 2 over the known distance L_2, one obtains the mode radius on the gain structure. A comparison with simulated mode radii then yields the dioptric power of the thermal lens.

The results of the thermal-lens measurement for the two gain structures soldered on a copper and a diamond heat spreader are shown in Figs. 8 and 9, respectively. In both cases, the heat sink temperature was 15 °C and the OC transmission was 0.8%. Since our measurement method is only applicable as long as the beam is in a fundamental transverse mode, the pump power at which the beam quality deteriorates is indicated in Figs. 8(a) and 9(a). The transverse intensity distribution was simultaneously displayed by the beam profiler which was used to measure the output beam radius. In addition, a separate M^2 measurement was done at the highest pump power of the measurement range which was used for the thermal-lens calculations in order to verify that the beam was indeed still close to single-transverse-mode at this point. The error bars in (b) and (c) of Figs. 8 and 9 are based on a measurement error of ± 2 mm for L_{meas}. The simulated values in Figs. 8(c) and 9(c) were calculated with the numerical model described in Section IV and will be discussed there.

In Fig. 9, the beam characteristics in the horizontal and vertical axis show a noticeable difference. We had to realign the cavity because the gain structure was changed between these measurements, which probably resulted in a slightly different position of the gain structure in the pump beam focus. In the measurement of Fig. 9 the pump spot most likely had a weakly elliptical profile.

The sample with the CVD diamond heat spreader shows better performance in terms of thermal lensing than the one with the copper heat spreader, which is a result of the reduced heating due to the higher thermal conductivity of diamond. For

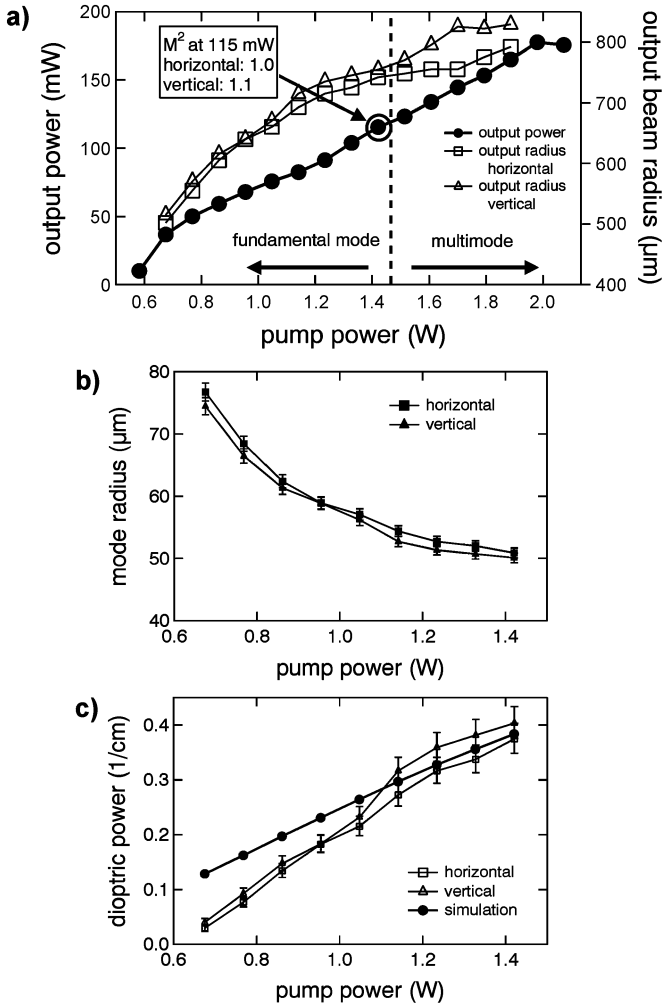

Fig. 8. Thermal lens measurement results in cw operation for the gain structure on a copper heat spreader. (a) Output power and output beam radius versus pump power. (b) Mode radius on the gain structure versus pump power. (c) Thermal lens dioptric power versus pump power. The output beam radius was measured at a distance $L_{\mathrm{meas}} = 121 \pm 2$ mm after the output coupler.

a given pump power and comparable output power, the thermal lens is weaker and the mode radius in the cavity is larger (e.g., dioptric power at 1.2 W of pump power is approximately 0.3 cm^{-1} for copper, whereas it is only around 0.2 cm^{-1} for diamond).

B. Cavity With a Flat Output Coupler

The thermal-lens measurements for a cavity design using the 200-mm curved OC gave us some important insights and allowed us to improve the average output power using a flat OC. The curved-OC cavity is capable of producing output powers of only about 100 mW in a single transverse mode in cw operation. Thus, the output power level in a mode-locked laser based on this cavity can be expected to be significantly lower due to the additional resonator losses introduced by the SESAM. Furthermore, the thermal lens is so strong that it is the dominant focusing element in the resonator (focal lengths of a few centimeters compared to a focal length of 10 cm for the 200-mm curved OC). For these reasons, a cavity design with a flat OC

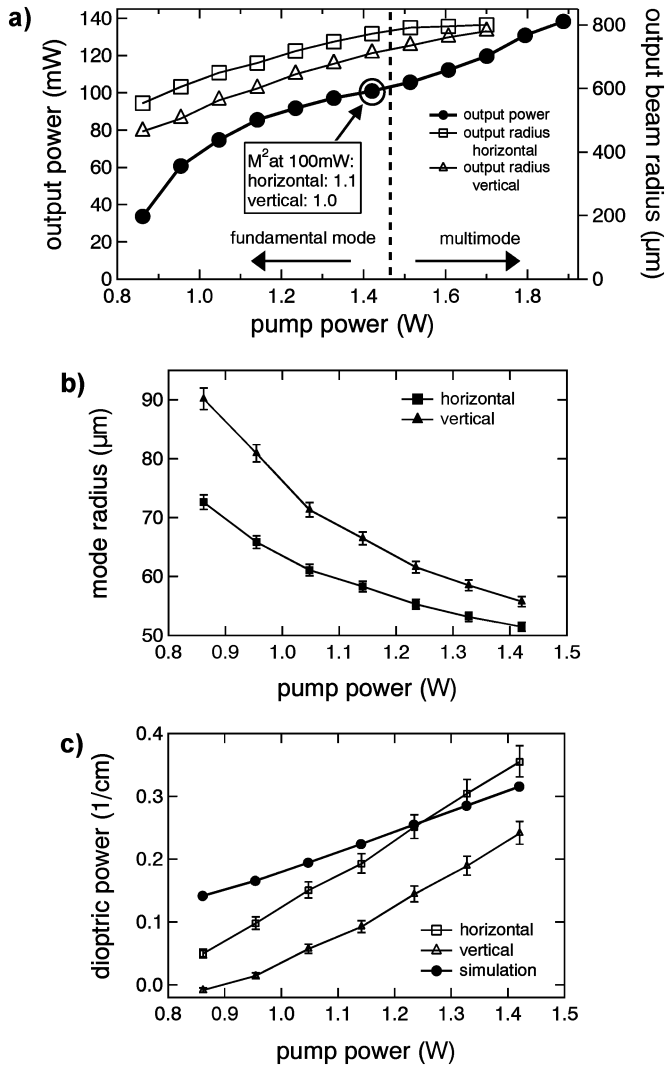

Fig. 9. Thermal lens measurement results in cw operation for the gain structure on a CVD diamond heat spreader. (a) Output power and output beam radius versus pump power. (b) Mode radius on the gain structure versus pump power. (c) Thermal lens dioptric power versus pump power. The output beam radius was measured at a distance $L_{\mathrm{meas}} = 127 \pm 2$ mm after the output coupler.

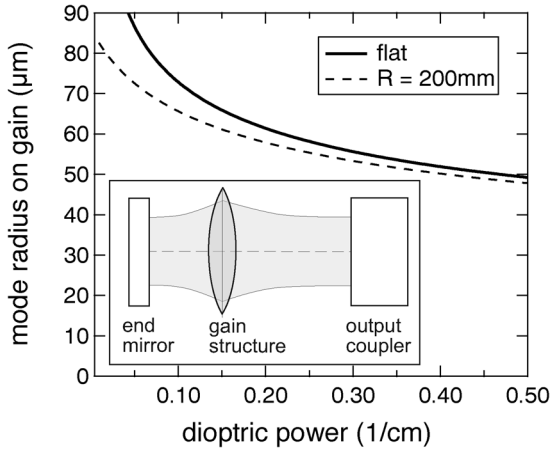

Fig. 10. Simulation of the influence of the thermal lens on the mode radius on the gain structure for a 50-GHz cavity using a flat output coupler (OC). The calculation for the curved OC with $R = 200$ mm is shown for comparison (dashed line). The inset shows the linear model of the cavity. The calculation was done for a wavelength of 960 nm and cavity arm lengths of 1 mm for end-mirror to gain and 2 mm for gain to OC.

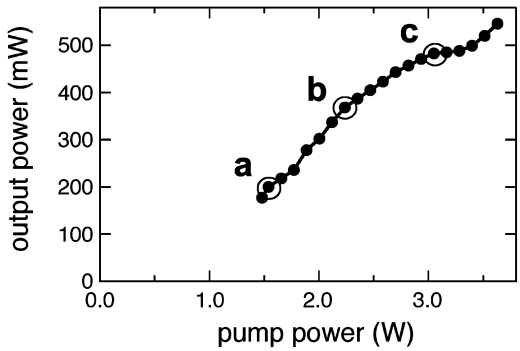

Fig. 11. Slope measurement in cw operation for the 50-GHz cavity using a flat output coupler with a transmission of 1.6%. An M^2 measurement as well as a thermal-lens measurement was done for each of the points a, b, and c.

was used in order to improve the cw output power. The beneficial increase in mode radius using a flat OC is illustrated in Fig. 10.

The 50-GHz flat-OC cavity was set up using a semiconductor Bragg reflector as the end mirror for cw operation. The OC transmission was 1.6%. The pump optics now had the aperture removed, resulting in a pump spot radius of about 70 μm. Because of its weaker thermal lensing, only the gain structure with the CVD diamond heat spreader was used from now on. The heat sink of the gain structure was held at 5 °C.

The result of the slope measurement is shown in Fig. 11. The characteristic abrupt turn-on behavior of a dynamically stable resonator is clearly visible. The laser can only start to lase at a pump power level where the thermal lens is strong enough to confine the mode to a radius comparable to the pump spot radius, since the fundamental mode will experience very high losses if it covers a significant amount of unpumped area in the periphery of the pump spot.

The thermal lens was measured for three points on the slope to get an impression of the mode radii and the dioptric powers of the thermal lens for the new pump spot and cavity configuration (see Fig. 11). We used the same technique as described before in Section III-A. The results are summarized in Table I for both the horizontal and the vertical axis. Since the M^2 was not unity for all measurements, the ray matrix calculations were done using an effective wavelength $\lambda_{\mathrm{eff}} = \mathrm{M}^2 \times \lambda$ in order to account for the increased divergence of the nonideal Gaussian beam. The results successfully demonstrate that this cavity is capable of producing output powers up to 370 mW in a nearly diffraction-limited beam with $\mathrm{M}^2 \leq 1.2$. Please note that an increase of the output coupling from 0.8% to 1.6% would also have increased the output power in the curved-OC cavity. The significantly improved output power of the flat-OC cavity results from the larger mode radius on the gain structure. This cavity was therefore used as the basis for the mode-locking experiments described in Section V.

IV. Numerical Model of the Thermal Lens

In order to gain a better understanding of the origin of the thermal lens in our VECSEL gain structures, we developed a numerical model which can calculate the approximate value of the thermal lens dioptric power that results from the temperature-dependence of the refractive index of the semiconductor

TABLE I
THERMAL-LENS MEASUREMENT OF THE FLAT-OUTPUT-COUPLER CAVITY

	a		**b**		**c**	
	p_{out} = 200 mW		p_{out} = 370 mW		p_{out} = 480 mW	
	hor.	vert.	hor.	vert.	hor.	vert.
M^2	1.1	1.1	1.2	1.0	1.7	1.7
w_{gain} (μm)	66 ± 2	68 ± 2	66 ± 2	57 ± 2	72 ± 2	70 ± 2
$f_{thermal}$ (cm)	5.4 ± 0.4	6.0 ± 0.3	4.3 ± 0.3	3.5 ± 0.2	3.2 ± 0.2	3.0 ± 0.2

TABLE II
THERMAL PROPERTIES OF MATERIALSTHERMAL-LENS MEASUREMENT OF THE FLAT-OUTPUT-COUPLER CAVITY

	thermal conductivity κ ($WK^{-1}m^{-1}$)	dn/dT (K^{-1})
GaAs	45	$2.8\cdot10^{-4}$
AlAs	91	$1.1\cdot10^{-4}$
$Al_{0.2}Ga_{0.8}As$	22.5	$2.5\cdot10^{-4}$
Cu	400	
CVD diamond	1800	
In	82	
Ti	22	
Pt	71	
Au	315	

materials. The lensing effects caused by carrier-induced refractive index changes in the gain structure as well as the SESAM are neglected here. A list of the material parameters used in our model is given in Table II. The dn/dT listed for $Al_{0.2}Ga_{0.8}As$ is a linear interpolation between the values for GaAs and AlAs for an Al content of 0.2. The thermal lens model can be subdivided into a thermal part and an optical part, which are described in the following.

A. Thermal Part

The thermal part of the model is based on a simplified analytical solution of the heat equation in VECSEL gain structures which has already been published in [12]. Refer to Fig. 12 for the definition of the geometry and symbols used in this context. We assume a one-dimensional (1-D) heat flow in the semiconductor structure and the solder junction, and a three-dimensional (3-D) heat flow into an infinite half-space of heat spreader material. The infinite boundaries of the heat spreader are held at a constant reference temperature $T_{\rm ref}$ (in practical terms: $T_{\rm ref}$ is the temperature of the heat sink which is held at a fixed value by a temperature controller). An infinitely thin heat source is located at the interface of the active region and the Bragg mirror, and it has a Gaussian transverse distribution with a $1/e^2$-radius w.

For such a Gaussian heat source, the 1-D temperature rise at the surface of a layer with thickness d of material with thermal conductivity κ is

$$\Delta T_{1-D}(r) = \frac{2P_{\rm heat}d}{\pi w^2\kappa}\exp\left(-2\frac{r^2}{w^2}\right). \tag{1.1}$$

It is also possible to obtain a closed-form analytical solution for the 3-D temperature rise at the surface of an infinite half-space with thermal conductivity κ and a Gaussian heat source [14]

$$\Delta T_{3-D}(r) = \frac{P_{\rm heat}}{\sqrt{2\pi}w\kappa}\mathrm{I}_0\left(\frac{r^2}{w^2}\right)\exp\left(-\frac{r^2}{w^2}\right) \tag{1.2}$$

where I_0 denotes the zeroth-order modified Bessel function of the first kind. Using these analytical expressions we can now calculate the temperature distribution at every coordinate (r, z) in the optical multilayer structure, which we divide into two regions I and II as indicated in Fig. 12.

At the surface of the heat spreader ($z = z_{\rm hs}$), the radial temperature distribution $T_{\rm hs}(r)$ is determined by using (1.2) to calculate the 3-D temperature rise with respect to the reference temperature $T_{\rm ref}$

$$T_{\rm hs}(r) = T_{\rm ref} + \Delta T_{3-D}(r). \tag{1.3}$$

For all regions on top of the heat spreader, the heat flow is one-dimensional. The 1-D temperature rise $\Delta T_{\rm solder}(r)$ across the solder junction, which comprises the metalization layers consisting of Ti–Pt–Au as well as the actual In solder layer, is calculated by adding up all the temperature rises across these individual metal layers calculated with (1.1)

$$\Delta T_{\rm solder}(r) = \sum_{\text{solder junction}} \Delta T_{1{\rm D},i}(r).$$

Likewise, the 1-D temperature rise $\Delta T_{\rm Bragg}(r)$ across the Bragg mirror is calculated as the sum of the 1-D temperature rises across all its individual layers

$$\Delta T_{\rm Bragg}(r) = \sum_{\text{Bragg mirror}} \Delta T_{1{\rm D},i}(r).$$

Inside region I ($0 \le z \le z_{\rm Bragg}$), the temperature distribution $T_{\rm I}(r, z)$ is obtained by linearly interpolating the 1-D temperature rise $\Delta T_{\rm Bragg}(r)$:

$$T_I(r,z) = T_{hs}(r) + \Delta T_{\rm solder}(r) + \Delta T_{\rm Bragg}(r)\times\frac{z}{d_{\rm Bragg}}. \tag{1.4}$$

Since no heat flow occurs inside region II ($z_{\rm Bragg} \le z \le z_{\rm top}$), the temperature distribution $T_{\rm II}(r, z)$ is independent of z

$$T_{II}(r,z) = T_{\rm hs}(r) + \Delta T_{\rm solder}(r) + \Delta T_{\rm Bragg}(r). \tag{1.5}$$

The analytical temperature model was checked against 3-D finite-element simulations using a heat source distributed over the active region. The lateral heat spreading in the Bragg mirror and the solder junction, which was ignored in the analytical model, results in only slight changes of the temperature profile. For a pump spot radius of 65 μm, a Bragg mirror thickness of 5.3 μm, a solder junction thickness of 5.5 μm, and a heating power of 0.7 W the maximum difference between the two temperature distributions was only 2.8 K, which is negligible compared to a maximum temperature rise of about 38 K in the center of the structure.

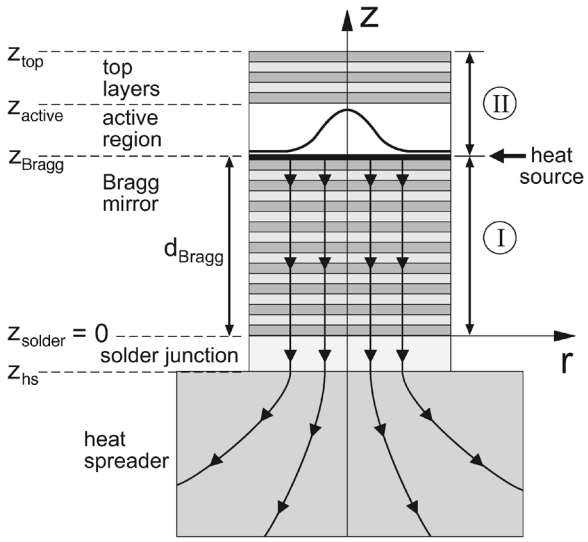

Fig. 12. Geometry for the thermal part of the thermal-lens model. A 1-D heat flow is assumed in the Bragg mirror and the solder junction, whereas a 3-D heat flow is assumed in the heat spreader. An infinitely thin heat source with a Gaussian transverse distribution is located at the interface between the Bragg mirror and the active region.

The heating power P_{heat} is equal to the incident pump power P_{pump} minus the sum of the reflected pump power P_{refl}, the laser output power P_{laser}, and the power P_{spont} radiated by spontaneous emission

$$\begin{aligned} P_{\mathrm{heat}} &= P_{\mathrm{pump}} - P_{\mathrm{refl}} - P_{\mathrm{laser}} - P_{\mathrm{spont}} \\ &= (1 - R_{\mathrm{pump}})P_{\mathrm{pump}} - P_{\mathrm{laser}} \\ &\quad - \eta_{\mathrm{rad}}\eta_{QD}(1 - R_{\mathrm{pump}})P_{\mathrm{pump,thres}} \end{aligned} \tag{1.6}$$

where $P_{\mathrm{pump,thres}}$ is the threshold pump power and R_{pump} is the pump reflection factor of the gain structure (this factor includes both the reflection at the nonperfect AR top section and the incomplete pump absorption after a double-pass through the active region. R_{pump} is around 15% for our gain structures). The calculation of the spontaneous-emission part [last term in (1.6)] assumes that the gain (and consequently the inversion) is clamped to a constant level above threshold. The radiated spontaneous emission power P_{spont} is then equal to the absorbed threshold pump power multiplied with the radiative efficiency η_{rad} of the QWs and a "quantum-defect" efficiency $\eta_{\mathrm{QD}} = \lambda_{\mathrm{pump}}/\lambda_{\mathrm{laser}}$ which accounts for the wasted power due to the difference between the pump and laser photon energies. The radiative efficiency of the QWs is assumed to be 70% in our calculations.

B. Optical Part

The optical part of the model is based on a matrix algorithm for optical multilayer structures. It takes a list of layer thicknesses and their associated refractive indices as its input and computes the complex reflectivity (magnitude and phase) at a given wavelength. The effect of the radial variation of the refractive indices in the optical multilayer structure on the phase profile of the reflected field is now approximated as follows: for N discrete values of r, one generates N modifications of the room-temperature multilayer structure in which the refractive index in each layer has been adjusted relative to its room-temperature value by using the linear temperature coefficients listed in Table II. This is possible because the temperature at every point (r, z) in the optical multilayer structure can be calculated using the temperature distributions $T_{\mathrm{I}}(r, z)$ and $T_{\mathrm{II}}(r, z)$ obtained with the thermal model. Within a layer, the temperature is assumed to be constant along the z-direction (the temperature in the middle of the layer is used as an average value). This allows to calculate the phase shift which a plane wave would experience at these discrete values of r, and thereby one obtains an approximation of the transverse phase profile which is imparted on the optical field as it is reflected by the optical multilayer structure. As might be expected, one obtains Gaussian-like phase profiles of the kind shown in Fig. 13. By taking the numerical second derivative at $r = 0$ (the coefficient of the leading-order term in the Taylor expansion), a parabolic approximation of the phase profile is calculated, which allows to extract the focal length f of the thermal lens by comparison with the phase profile of a wave front after transmission through an ideal thin lens [15]

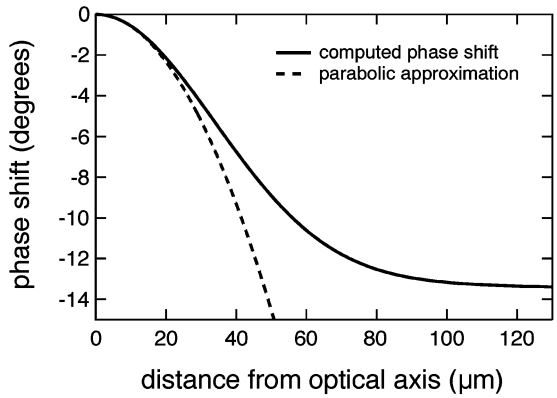

Fig. 13. Phase shift which is imparted on a plane wave front upon reflection from the gain structure as a function of distance r from the optical axis, relative to the phase shift on the optical axis. The solid line was calculated with the numerical model for a pump spot radius of 65 μm, a heating power of 0.7 W, and a gain structure which is soldered to a CVD diamond heat spreader. The calculated total temperature rise in the center of the pump spot was 38 K. The dashed line shows the parabolic approximation of this phase profile and corresponds to a focal length of 3.2 cm.

$$\varphi(r) = -\frac{k_0}{2f}r^2 \tag{1.7}$$

where k_0 is the vacuum wave-vector at the wavelength of interest. Looking at Fig. 13, it is evident that the thermal lens introduces considerable aberrations, since the parabolic approximation already deviates strongly from the actual phase profile at the $1/\mathrm{e}^2$-radius w of the Gaussian pump intensity distribution.

C. Comparison With Measurements

The calculated values of the dioptric power of the thermal lens are plotted along with the measured values in Figs. 8(c) and 9(c). For every value of pump power, the heating power was calculated using (1.6). The agreement between the calculated and the measured values is good for higher pump powers; however, they differ by a factor of two or more at low pump powers. In this context, it is important to keep in mind the limitations of the model. It was observed in Fig. 13 that the parabolic approximation of the phase profile is only valid for radii smaller than the pump spot radius w, which was around 65 μm in these mea-

surements. For low pump powers and weak thermal lensing, the mode radius on the gain structure is significantly larger than this [around 70–80 μm, see Figs. 8(b) and 9(b)], and for these conditions it is not surprising that the leading-order effect of the parabolic component of the phase profile will not be sufficient for a realistic description of the lensing effect. For higher pump powers (above $\approx$ 1 W for the copper-heat-spreader sample and above $\approx$ 1.2 W for the diamond-heat-spreader sample), the mode radius on the gain structure reaches values around 60 μm or less, where the approximation of the phase profile by the parabolic term starts to become valid.

When used under conditions where the laser mode covers a region comparable to or smaller than the pump spot size, the numerical model achieves a satisfactory level of accuracy and can be used in the practical design and optimization of laser cavities. Since it calculates the full phase profile, it also contains all the information about the aberrations of the thermal lens and can potentially be extended to more sophisticated optical modeling such as the calculation of diffraction losses which arise due to the higher order terms in the phase profile.

V. Passive Mode Locking

Based on our previous discussions in Section III, a passively mode-locked VECSEL was built using a cavity with a flat OC and a gain structure with a CVD diamond heat spreader. The OC transmission was kept at 1.6% and the high-reflecting Bragg mirror was replaced with a low-F_{sat} QD SESAM. A 25-μm-thick uncoated fused-silica etalon was inserted into the cavity for wavelength tuning and dispersion control.

The low-F_{sat} QD SESAM used in these experiments was a resonant design (resonance wavelength around 940 nm). It has a 30-pair AlAs–GaAs Bragg mirror and it contains a single absorber layer of self-assembled InAs QDs placed in the maximum of the standing-wave pattern. It was grown by solid-source molecular beam epitaxy (MBE) at 580 °C, with the exception of the absorber layer, which was grown at a lower temperature around 360 °C in order to introduce crystal defects acting as recombination centers and thereby enabling fast recovery times. This SESAM is similar in design and growth parameters to the QD SESAM previously described in [9]; however, the resonance wavelength was shifted from 955 to 940 nm resulting in a smaller modulation depth. At the laser wavelength we measured a linear reflectivity of 99.2%, which implies a modulation depth below 0.8%.

By tuning the wavelength of the laser with the etalon and by varying the pump power level, mode locking was achieved in the wavelength range around 957–960 nm. The pulse characterization of our best result is shown in Fig. 14. The average output power was 102 mW at a pump power of 3.7 W. The heat sink of the gain structure was held at 5°C. The 3.3-ps pulses are nearly transform-limited, with a spectral FWHM of 0.36 nm and a time-bandwidth product of 0.39. The output beam was linearly polarized in the horizontal direction and the beam quality was close to the diffraction limit, with an M^2 of 1.25 and 1.13 in the horizontal and vertical axes.

The mode radii on the gain structure and on the SESAM were approximately 62 μm, from which one can calculate the intracavity pulse fluence to be around 1.1 μJ/cm^2. The mode

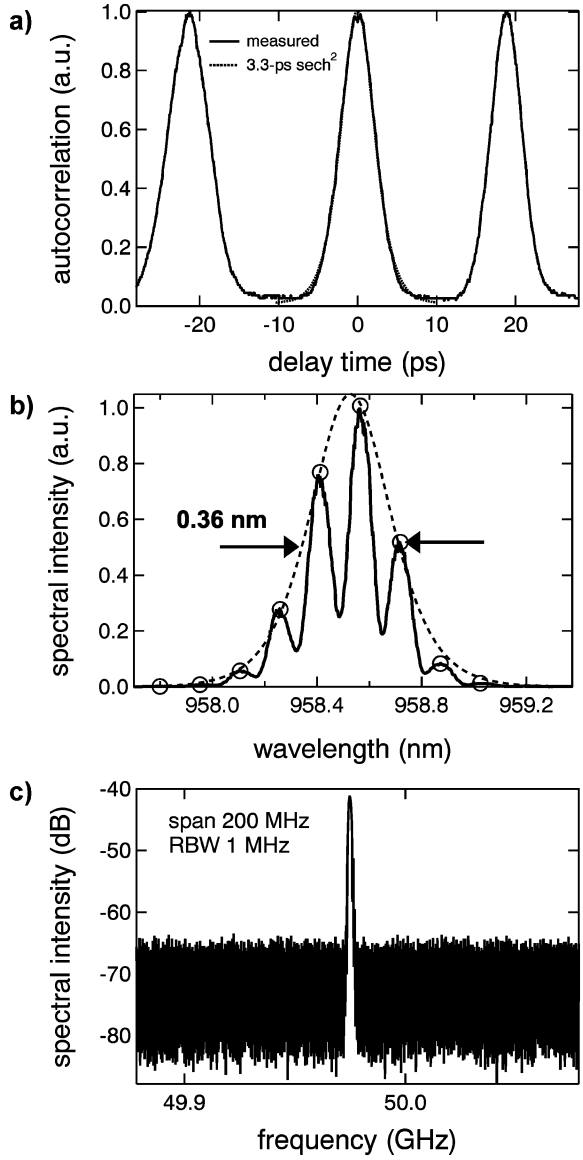

Fig. 14. Pulse characteristics of the 50-GHz mode-locked VECSEL with 102-mW average output power. (a) Autocorrelation of the pulse train. The fit corresponds to an ideal 3.3-ps sech^2 pulse. (b) Optical spectrum. The longitudinal modes of the laser are resolved and their intensities can be fitted with a sech^2 envelope with a FWHM of 0.36 nm. (c) RF spectrum of the laser output measured with a fast photodiode.

size in the cavity was determined by the method outlined in Section III (measurement of the output beam radius). The corresponding focal length of the thermal lens was calculated to be (3.2$\pm$ 0.3) cm.

The long-term stability of the mode locking was limited by the fairly strong degradation of this particular gain structure sample. The output power decreased noticeably during the beam profile (M^2) measurement, which took about 15 min. At the end of the measurement the laser was still mode-locked, but the output power had dropped to about 80 mW and the pulse quality had deteriorated somewhat. Other samples of this very same gain structure, mounted on copper heat spreaders, had lased for about 100 h until the output power dropped to 50% of its initial value. We suspect that a flawed solder junction in this device is the reason for the unusually fast degradation, due to adhesion problems which had been observed during the metaliza-

tion process prior to soldering. By improvement of the soldering and processing it should be possible to eliminate these problems, since high-performance VECSEL gain structures soldered to CVD diamond heat spreaders exist and are already incorporated into commercial laser products [16].

Mode locking experiments were also conducted using a lower output-coupler transmission of 0.8%. The maximum achievable output powers were lower, our best result being 42 mW at a pump power of 2.4 W. The pulse characteristics were very similar to those of the 102-mW result, with a pulse duration of 3.1 ps and a time-bandwidth product of 0.39. The intracavity pulse fluence was determined to be about 0.9 μJ/cm^2 in that case, indicating that this combination of gain structure and SESAM seem to work best at pulse fluences around 1 μJ/cm^2.

VI. Conclusion

We have successfully demonstrated that the concept of the optically-pumped passively mode-locked VECSEL is suitable for the realization of picosecond laser sources in the 100-mW power class at high repetition rates up to 50 GHz. This is two orders of magnitude more output power directly from a laser oscillator (i.e. without subsequent amplifier stages) than what can be obtained with the currently dominant technology based on edge-emitting semiconductor lasers. Despite their high performance in terms of output power, pulse characteristics and beam quality, the level of complexity and total system cost associated with optical pumping and the alignment of folded cavities currently limits the practical applicability of optically-pumped passively mode-locked VECSELs to scientific applications or low-volume markets. The rapid progress in the field of passively mode-locked VECSELs in recent years gives us confidence that the integration of the absorber into the gain structure can be achieved even though it represents a challenging task in terms of epitaxial growth. In addition, electrical pumping of these semiconductor lasers would further reduce the overall system complexity. The experimental work presented here as well as in [9] seems to indicate that no fundamental limitations with regard to the underlying physics must be expected: The quantum-dot absorber material has a sufficiently low saturation fluence to induce stable mode locking with identical mode areas on gain and absorber, and the clearly separated 3.3-ps pulses in the 50-GHz pulse train show that the temporal dynamics of the semiconductor gain and absorber medium can most likely support pulse formation at even higher repetition rates. This would yield low-cost and rugged monolithic pulsed laser sources with impressive specifications concerning repetition rate and output power which would fill a gap in the performance spectrum of today's laser technology.

References

[1] F. Kuznetsov, F. Hakimi, R. Sprague, and A. Mooradian, "High-power (>0.5-W CW) diode-pumped vertical-external-cavity surface-emitting semiconductor lasers with circular TEM$_{00}$ beams," *IEEE Photon. Technol. Lett.*, vol. 9, no. 8, pp. 1063–1065, Aug. 1997.

[2] S. Hoogland, S. Dhanjal, A. C. Tropper, S. J. Roberts, R. Häring, R. Paschotta, and U. Keller, "Passively mode-locked diode-pumped surface-emitting semiconductor laser," *IEEE Photon. Technol. Lett.*, vol. 12, no. 9, pp. 1135–1138, Sep. 2000.

[3] U. Keller, D. A. B. Miller, G. D. Boyd, T. H. Chiu, J. F. Ferguson, and M. T. Asom, "Solid-state low-loss intracavity saturable absorber for Nd:YLF lasers: an antiresonant semiconductor Fabry–Perot saturable absorber," *Opt. Lett.*, vol. 17, pp. 505–507, 1992.

[4] U. Keller, K. J. Weingarten, F. X. Kärtner, D. Kopf, B. Braun, I. D. Jung, R. Fluck, C. Hönninger, N. Matuschek, and J. Aus der Au, "Semiconductor saturable absorber mirrors (SESAMs) for femtosecond to nanosecond pulse generation in solid-state lasers," *IEEE J. Sel. Topics Quantum Electron.*, vol. 2, no. 3, pp. 435–453, Sep. 1996.

[5] A. Aschwanden, D. Lorenser, H. J. Unold, R. Paschotta, E. Gini, and U. Keller, "2.1-W picosecond passively mode-locked external-cavity semiconductor laser," *Opt. Lett.*, vol. 30, pp. 272–274, 2005.

[6] ——, "10-GHz passively mode-locked surface emitting semiconductor laser with 1.4-W average output power," *Appl. Phys. Lett.*, vol. 86, 2005, 131102.

[7] A. C. Tropper, H. D. Foreman, A. Garnache, K. G. Wilcox, and S. H. Hoogland, "Vertical-external-cavity semiconductor lasers," *J Phys. D: Appl. Phys.*, vol. 37, pp. R75–R85, 2004.

[8] K. Jasim, Q. Zhang, A. V. Nurmikko, E. Ippen, A. Mooradian, G. Carey, and W. Ha, "Picosecond pulse generation from passively mode-locked vertical cavity diode laser at up to 15 GHz pulse repetition rate," *Electron. Lett.*, vol. 40, pp. 34–35, 2004.

[9] D. Lorenser, H. J. Unold, D. J. H. C. Maas, A. Aschwanden, R. Grange, R. Paschotta, D. Ebling, E. Gini, and U. Keller, "Towards wafer-scale integration of high repetition rate passively mode-locked surface-emitting semiconductor lasers," *Appl. Phys. B*, vol. 79, pp. 927–932, 2004.

[10] A. Bhatnagar and D. A. B. Miller, "Optical interconnection and clocking for electronic chips," in *Proc. 8th World Multiconf. Systemics, Cybernetics, Informatics*, Orlando, FL, 2004 [Online]. Available: http://www-ee.stanford.edu/~dabm/276.pdf

[11] M. J. Kobrinsky, B. A. Block, J.-F. Zheng, B. C. Barnett, E. Mohammed, M. Reshotko, F. Robertson, S. List, I. Young, and K. Cadien, "On-chip optical interconnects," *Intel Technol. J.* vol. 8, no. 2, 2004 [Online]. Available: http://www.intel.com/technology/itj/2004/volume08issue02/art05_on-chip/p01_abstract.htm

[12] R. Häring, R. Paschotta, A. Aschwanden, E. Gini, F. Morier-Genoud, and U. Keller, "High-power passively mode-locked semiconductor lasers," *IEEE J. Quantum Electron.*, vol. 38, no. 9, pp. 1268–1275, Sep. 2002.

[13] A. E. Siegman, *Lasers*. Mill Valley, CA: University Science Books, 1986.

[14] G. T. Martin and H. F. Bowman, "The temperature distribution in a semi-infinite body due to surface absorption of laser radiation," *Int. Comm. Heat Mass Transfer*, vol. 17, pp. 93–104, 1990.

[15] D. Marcuse, *Light Transmission Optics*. New York: Van Nostrand, 1972.

[16] J. Chilla, S. Butterworth, A. Zeitschel, J. Charles, A. Caprara, M. Reed, and L. Spinelli, "High power optically pumped semiconductor lasers," in *Photonics West 2004, Solid State Lasers XIII: Technology and Devices, Proc. SPIE 5332*, 2004, pp. 143–150.

Dirk Lorenser was born in Asuncion, Paraguay, in 1974. He received the M.Sc. degree in physics (Dipl. Phys.) from the University of Bonn, Bonn, Germany, in 2000 and the Ph.D. degree in physics from ETH Zurich, Switzerland, in 2006.

His area of specialization is experimental work related to electromagnetic fields, RF/microwave technology, and electronics. In 2001, he joined the Institute of Quantum Electronics, ETH Zurich, where he has been involved in the development of multigigahertz passively mode-locked vertical-external-cavity surface-emitting semiconductor lasers.

Deran J. H. C. Maas was born in Maastricht, The Netherlands, in 1979. He received the M.Sc. degree in electrical engineering (*cum laude*) from the Eindhoven University of Technology, Eindhoven, The Netherlands in 2003.

In 2004, he joined the Institute of Quantum Electronics, ETH Zurich, Switzerland, where he is engaged in the research and development of high repetition rate passively mode-locked semiconductor lasers. His research interests are in the field of quantum electronics, laser physics, telecommunication technology, and information theory.

Heiko J. Unold was born in Aalen, Germany, on March 25, 1973. He received the Dipl.-Ing. degree in electrical engineering from the University of Ulm, Ulm, Germany, in 1998 and the Dr.-Ing. degree in high-power single-mode VCSEL design and fabrication at the Department of Optoelectronics, University of Ulm.

Currently, he is working on passively mode-locked VECSELs at the Swiss Federal Institute of Technology (ETH), Zürich, Switzerland.

Aude-Reine Bellancourt was born in Rouen, France, in 1982. She received the Diploma of Physicist Engineer degree from Ecole Supérieure d'Optique, Orsay, France, in 2004. During her Diploma thesis work at Toptica Photonics in Munich, Germany, she worked on the characterization of picosecond pulses produced by laser diode systems.

Since 2005, she has been part of the research group of U. Keller at ETH, Zurich, Switzerland, and is in charge of the design, processing and characterization of VECSELs in order to build compact mode-locked laser sources with multigigahertz repetition rates.

Benjamin Rudin was born in Thalwil, Switzerland, in 1978. He received the Diploma degree in experimental physics from the Swiss Federal Institute of Technology (ETH), Zurich, Switzerland.

He joined the Institute of Quantum Electronics, ETH, in 2005. His research is focused on mode-locked vertical-external-cavity surface-emitting lasers.

Emilio Gini was born in Davos, Switzerland, on September 20, 1961. He received the degree in physics and the Ph.D. degree in dry etched InGaAsP/InP passive optical waveguide devices from the Swiss Federal Institute of Technology (ETH), Zurich, Switzerland in 1986 and 1997, respectively.

From 1988 to 2000, he was with the Institute of Quantum Electronics, Zurich, where he worked on the growth of III-V semiconductor compounds by LP-MOVPE and dry etching techniques for the fabrication of optoelectronic integrated circuits (OEICs). In 2000, he joined the FIRST Center for Micro- and Nanosciences, Zurich. He is responsible for the MOVPE growth of III-V compound semiconductor-based optoelectronic devices. He has written and coauthored about 50 scientific papers and conference contributions.

Dirk Ebling received the M.Sc. and Ph.D. degrees in chemistry from the University of Duesseldorf, Duesseldorf, Germany. His thesis research concerned the fabrication of submicrometer structures in alumina and their electrical and optical properties.

After graduation in 1991, his research focused on the characterization and growth of compound semiconductor materials at the University of Freiburg, Germany. Beside the development of X-ray radiation detectors his research was focused on the development of advanced ultraviolet sensors from wide band gap materials and on the MBE growth and analysis of group V alloys in III/V semiconductors. Since 2001, he has been involved in the growth and development of optical devices from III/V materials for laser applications at the FIRST Center for Micro- and Nanosciences, ETH, Zurich, Switzerland.

Ursula Keller (SM'02) was born in Zug, Switzerland, in June 1959. She received the Diploma in physics from the Federal Institute of Technology (ETH), Zurich, Switzerland, in 1984 and the M.S. and Ph.D. degrees in applied physics from Stanford University, Stanford, CA, in 1987 and 1989, respectively. Her Ph.D. research was in optical probing of charge and voltage in GaAs integrated circuits and in low-noise ultrafast laser systems.

From late 1984 to 1985, she worked on optical bistability at Heriot-Watt University, Edinburgh, Scotland. For her first year at Stanford, she held a Fulbright Fellowship and for the following year she was an IBM Predoctoral Fellow. In 1989, she became a Member of Technical Staff (MTS) at AT&T Bell Laboratories, Holmdel, NJ, where she conducted research on photonic switching, ultrafast laser systems, and semiconductor spectroscopy. In March 1993, she was appointed as an Associate Professor and in October 1997 she became a Full Professor in the Physics Department at ETH. Her current research interests are in ultrafast lasers, high harmonic generation and attosecond science, ultrafast spectroscopy, and novel devices for applications in optical information processing and communication. She has published more than 240 peer-reviewed journal papers and 11 book chapters and she holds or applied for 17 patents.

Prof. Keller received the Carl Zeiss Research for her pioneering work in novel modelocking and Q-switching techniques using semiconductor saturable absorber mirrors (SESAMs) in 1998. In 2000, she was elected for the LEOS Distinguished Lecturer Award for modelocked solid-state lasers. In 2003, she became an OSA Fellow for pioneering contributions to the generation of few-optical-cycle laser pulses and applications and the development of semiconductor saturable absorber mirrors. In 2004, she received the First-Place Award of the Berthold Leibinger Innovation Prize and in 2005 the Philip Morris Research Award. She is an elected foreign member of the Royal Swedish Academy of Sciences, a fellow of the Optical Society of America (OSA), and a member of the European Physical Society (EPS), the Swiss Physical Society (SPS), and the Swiss Academy of Technical Sciences (SATW).